ACS MATERIALS Au
AN OPEN ACCESS JOURNAL OF THE AMERICAN CHEMICAL SOCIETY

pubs.acs.org/materialsau
Article

Multijet Gold Nanoparticle Inks for Additive Manufacturing of Printed and Wearable Electronics

Tony Valayil Varghese,* Josh Eixenberger, Fereshteh Rajabi-Kouchi, Maryna Lazouskaya, Cadré Francis, Hailey Burgoyne, Katelyn Wada, Harish Subbaraman, and David Estrada*

Cite This: ACS Mater. Au 2024, 4, 65−73
Read Online

ACCESS | Metrics & More | Article Recommendations | Supporting Information

ABSTRACT: Conductive and biofriendly gold nanomaterial inks are highly desirable for printed electronics, biosensors, wearable electronics, and electrochemical sensor applications. Here, we demonstrate the scalable synthesis of stable gold nanoparticle inks with low-temperature sintering using simple chemical processing steps. Multiprinter compatible aqueous gold nanomaterial inks were formulated, achieving resistivity as low as $\sim 10^{-6}$ Ω m for 400 nm thick films sintered at 250 °C. Printed lines with a resolution of <20 μm and minimal overspray were obtained using an aerosol jet printer. The resistivity of the printed patterns reached $\sim 9.59 \pm 1.2 \times 10^{-8}$ Ω m after sintering at 400 °C for 45 min. Our aqueous-formulated gold nanomaterial inks are also compatible with inkjet printing, extending the design space and manufacturability of printed and flexible electronics where metal work functions and chemically inert films are important for device applications.

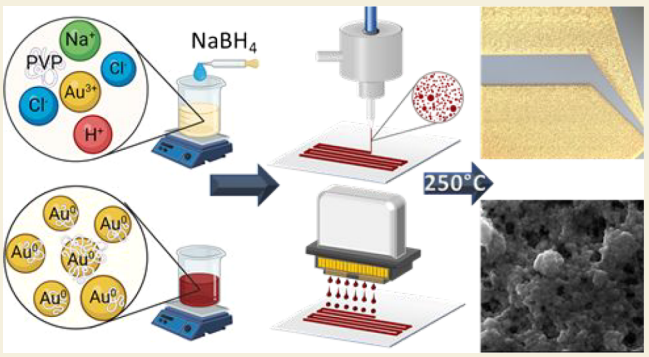

KEYWORDS: *additive manufacturing, gold nanoparticles, inkjet printing, aerosol jet printing, printed electronics*

INTRODUCTION

Additive manufacturing (AM) is a rapidly growing market that provides efficient and cost-effective solutions for the manufacturing industry, enabling the fabrication of novel materials and devices.[1−7] However, most AM tools, especially ones aimed at utilizing AM for electronics and sensors, are limited to a handful of conductive nanomaterial-based inks, creating a strong demand for a new generation of inks. Implementation of AM tools for the fabrication of flexible hybrid electronics, healthcare electronics, and consumer electronics requires environmentally and biofriendly conductive nanoparticle inks which can be sintered at a lower temperature to be compatible with the desired substrate while still achieving bulk-like performance.[8] Printing technologies are broadly categorized as contact and contactless methods.[9,10] Contact printing, also known as transfer printing, can be compatible with roll-to-roll (R2R) technologies which directly transfer ink onto substrates. Even though contact printing involves high costs, extended setup, and significant nanomaterial usage, it is suitable for high-volume production.[11,12] In contrast, contactless printing employs nozzles to accurately deposit ink without substrate contact, reducing nozzle contamination and materials usage. Also, noncontact methods enable digital printing and offer design flexibility with high resolution. Unlike contact printing, noncontact techniques facilitate diverse pattern printing without hardware modifications, making them efficient for prototyping. Notable noncontact methods include inkjet and aerosol jet printing. Inkjet excels in printing planar electronic components with a printing resolution near 50 μm. Aerosol jet printing can be done both in-plane and conformally on three-dimensional (3D) objects with a finer resolution of 10 μm as compared to inkjet printing.

In general, additive manufacturing of functional nanomaterials offers a promising strategy for the scalable production of printed and flexible electronics by enabling rapid prototyping and design flexibility. Compared to conventional manufacturing, contactless direct jet printing technologies such as inkjet printing and aerosol jet printing allow for high-precision printing with easy customization, reduce material waste, offer rapid production, and are scalable via R2R manufacturing.[13] Substantial progress has been made in optimizing and understanding the fluid dynamics of material jetting printers, particularly for inkjet printing.[14−17] Hence, most commercially available inks are finely tuned for inkjet printing, with no inks available in the market that are reported to be formulated for compatibility across different material jetting platforms. Even when looking specifically at inkjet and aerosol jet printers, the

Received: July 18, 2023
Revised: October 1, 2023
Accepted: October 4, 2023
Published: November 2, 2023

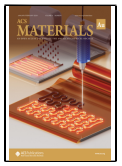

most used jetting platforms, inks, are formulated specifically for only one type of printer. This lack of cross-platform compatible inks limits applications of these AM technologies and requires different inks to be purchased or reformulated in-house to be cross-platform compatible, creating higher costs and increased labor. Additionally, most nanomaterial-based inks typically contain toxic organic solvents and a high concentration of surfactants and/or dispersing agents to maintain particle stability, enable higher nanoparticle loading, and match the rheological requirements of the printers.[18,19] The presence of such additives in the ink creates postprocessing challenges. For example, high-temperature thermal sintering can remove the additives, but their thermal decomposition creates highly porous structures.[20−22] This high-temperature thermal sintering requirement also limits the choice of substrates that are compatible with the required sintering temperatures, typically resulting in polyimide as the preferred material for flexible applications.

AM of electronics can be a complementary technique for multiple cleanroom fabrication processes. While printing technologies cannot fabricate devices in the nanoscale scale-like photolithography processes, utilizing AM to screen new materials and their properties can accelerate discoveries that can be translated to more traditional semiconductor processes.[23] AM can also fabricate electronic devices that do not require small feature sizes while still taking advantage of different nanomaterial properties. In this regard, there have been various types of laboratory-scale conductive inks developed to meet this growing demand including metal nanoparticles (silver, copper, gold),[24,25] carbon allotropes[26,27] (graphene, CNTs, etc.), MXenes ($Ti_2C_3T_x$),[28] and conductive polymers (PEDOT:PSS).[29,30] Most ink development for AM tools has concentrated on ink jet printers, with silver nanoparticle inks being the favored choice due to their low production cost and high electrical conductivity. However, silver ink is limited by its low chemical stability and high diffusion of silver ions in the presence of electric fields, low metal work functions, and elevated temperature limits, which restrict its use in printed electronics, energy storage, and bioelectronic applications. Gold nanoparticle inks offer a solution to these constraints with their superior chemical stability, biocompatibility, and ability to withstand extreme chemical and thermal conditions.

In this work, we have created a cost-effective and easily scalable method of synthesizing gold nanoparticle inks that can be sintered at low temperatures. By considering the rheological needs of various printing platforms, we have made our formulations suitable for use with multiple printers, allowing for effortless interchangeability. This procedure utilizes a room-temperature solvent reduction process to create surfactant coated gold nanoparticles and a multistep washing procedure to optimize the concentration of surfactants in the ink. A detailed characterization of the ink formulation and rheological properties was conducted to ensure that our gold nanoparticle-based ink is cross-platform compatible with inkjet and aerosol jet printing. Furthermore, we use our aqueous-based multijet formulation to print gold structures on a silicon wafer and polyimide substrates to obtain high-performing gold interconnects and test structures. This study showcases the capabilities of our water-based gold inks that can be used for printing interconnects, flexible electronics, and wearable healthcare devices. It also allows users to utilize the advantages of various platforms through a hybrid manufacturing process. This approach can blend the fast production of large features with ink jet technology and the precise capabilities of the aerosol jet technology.

EXPERIMENTAL METHODS

Gold Nanoparticle Synthesis

Hydrogen tetrachloroaurate(III) hydrate ($HAuCl_4.3H_2O$, 99.999% purity, Sigma-Aldrich), 10 kDa polyvinylpyrrolidone (PVP, Alfa Aesar), 98% sodium tetrahydroborate ($NaBH_4$, 98%, Alfa Aesar), sodium hydroxide pellets (NaOH, 95−100.5% Macron), and ethylene glycol (EG, VWR) were purchased from commercial sources and used without further purification. Additionally, a 2.2 M stock solution of $NaBH_4$ was prepared with the addition of 0.500 g of $NaBH_4$ to 6 mL of nanopure water (18 MΩ) with the pH adjusted to a pH of 12 with NaOH. Both solutions were used without further purification or dilution. A room-temperature wet chemical reduction process was used to obtain PVP-capped Au nanoparticles (PVP-AuNPs). 2 g of $HAuCl_4{\cdot}3H_2O$ was dissolved in 2 L of nanopure water containing 4 g of dissolved PVP, followed by manual dropwise addition of 6 mL of stock $NaBH_4$ using a disposable pipet to form PVP-AuNPs. The resulting suspension was allowed to stir vigorously for 12 h, and this process was repeated until the desired amount of PVP-AuNPs was obtained. The removal of excess capping agent and reaction byproducts was performed through multiple washing steps using cross-flow filtration and centrifugation. In order to remove the excess PVP presented in the concentrated PVP-AuNPs solution, a dilute concentration of sodium borohydride (7 mg/mL) was added at a ratio 1:3 to the solution and stirred continuously for 12 h. The resulting solutions were washed multiple times using nanopure water and concentrated to obtain a water dispersed PVP-AuNPs solution. Stable 1−5 wt % of AuNP-containing inks were prepared by the addition of ethylene glycol and ethanol into the water-gold nanoparticle solution.

AuNP Characterization

Absorbance spectra were collected using a Cary 5000 UV−vis−NIR spectrophotometer using 4.5 mL disposable cuvettes (Fisher Scientific). Absorbance spectra were collected from 400 to 750 nm with a 0.500 nm step size and 0.100 dwell time. To understand and determine ink concentrations after processing, we recorded spectra for six different concentrations of gold nanoparticles suspended in water. A linear correlation between absorbance and concentration was determined by plotting the peak absorbance intensity of the surface plasmon resonance peak of the gold at 532 nm against the concentrations used.

Thermogravimetric analysis (TGA) utilized a Netzsch STA449F1 TGA-DSC to determine the amount of PVP retained on the particles from the synthesis procedure and after subsequent washing steps using sodium borohydride (7 mg/mL) to remove the bound PVP. To prepare the samples for TGA, 50 μL of the gold ink was pipetted into the alumina crucibles and dried in an oven at 70 °C for 1 h. This was repeated until at least 5 mg of the gold NP sample was obtained in the alumina crucible. The sample was then placed into the TGA chamber, and the sample was heated to 700 °C with a heating rate of 10 °C per minute in a nitrogen atmosphere.

Transmission electron microscopy (TEM) was performed using a JEOL JEM-2100 HR analytical transmission electron microscope to obtain the particle size distribution and observe the morphology of the gold nanoparticles. The gold prints were analyzed with FEI Teneo SEM with the T2 secondary electron detector for secondary electron SEM images to analyze the morphology of the printed samples. Images were collected with a working distance of 2 mm, an accelerating voltage of 20 kV, and a current of 0.4 nA.

AuNP Ink Characterization

The viscosity of the inks was determined with a DVNext torque meter (AMETEK Brookfield, Middleborough, Massachusetts, USA) with a CP-40 spindle. A 1 mL sample of ink was placed in a stationary sample plate, and the measurement was conducted at room

https://doi.org/10.1021/acsmaterialsau.3c00058
ACS Mater. Au 2024, 4, 65−73

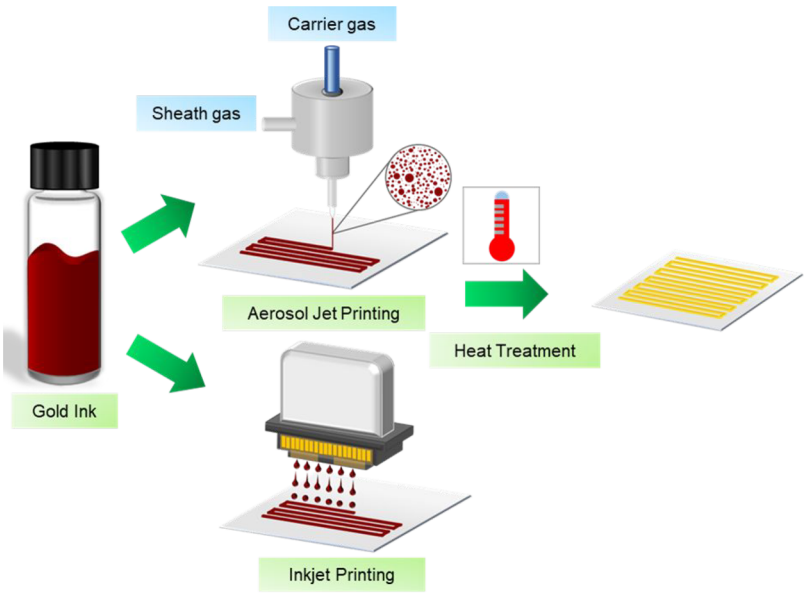

Figure 1. Schematic illustration of multiprinter compatible aqueous gold nanomaterial inks for printed electronics.

temperature (22 °C) by gradually increasing the rotation speed from 10 to 150 rpm with a step size of 10 rpm at a duration of 30 s. The surface tension and contact angle of the formulated ink were determined with a Theta Flex optical tensiometer (Biolin Scientific AB, Gothenburg, Sweden) in pendant drop and sessile drop tests, respectively. OneAttension software was used to analyze the acquired data. Surface tension was determined by generating a 5 μL droplet of the ink and capturing the images with a camera (resolution of 5 MP) at LED-based homogeneous background lighting for 10 s with 33 fps. The contact angle of our synthesized gold ink is directly measured via the sessile drop technique using the classical Young–Laplace equation on various substrates including tattoo paper, Kapton, polyethylene terephthalate (PET), and PEL60 substrates. A 10 μL droplet of the ink was deposited onto substrates, and the contact angle was recorded for 10 s at room temperature and in open air.

Gold Nanoparticle Printing

Figure 1 illustrates an overview of the multijet compatible gold ink formulation for both aerosol jet and ink jet printers. Au electrodes were printed utilizing a Dimatix inkjet printer (DMP-2850, Fujifilm, NY, USA). For the printing of the Au electrodes, the Samba cartridge (12 nozzle-cartridge that generates 10 pL droplets) was loaded with freshly prepared Au ink and heated to 40° °C. Kapton substrate (Dupont, Wilmington, DE) was placed on the printer platen and heated to 55 °C to ensure rapid drying of the printed ink. Furthermore, 3 nozzles were used to print the selected pattern, and the waveform recommended for Samba cartridge with the voltage around 26–28 V was used to generate the drops with a spacing of 10 μm. Five layers with an interlayer delay of 120 s were printed to reach the optimal thickness of the Au electrodes. Furthermore, the gold inks were also printed utilizing an Optomec Aerosol Jet Printer (Optomec 200, Optomec, NM, USA). The printing was performed by utilizing an ultrasonic atomizer with varying nozzle diameters. Printing parameters for a 300 μm nozzle are listed in the Results and Discussion (Table 1).

Table 1. Aerosol Jet Printing Parameters

parameters	values
nozzle diameter (μm)	300
sheath gas flow (sccm)	45–60
UA atomizer flow (sccm)	28–35
UA atomizer current (A)	0.3–0.45
platen temperature (° C)	65–70
water bath temperature (° C)	25–30
process speed (mm/s)	1–10

RESULTS AND DISCUSSION

Gold nanoparticles were synthesized by using a modified burst reduction method in the presence of PVP. Figure S1 shows a schematic representation of the reduction process. Multiple batches of nanoparticles were produced, washed, concentrated, and then combined to obtain enough product to formulate printable inks. PVP was selected as a capping agent as it has been extensively used in the synthesis of Au NPs to control size, shape, and improve stability in the desired solvent system.[31] Other strategies to stabilize NPs have been utilized, including citrate, cetyltrimethylammonium bromide (CTAB), polyethylene glycol (PEG), and biomolecules.[32] While these other methods have certain advantages, PVP was chosen as it can also promote the adhesion of the nanoparticles to various substrates used for printed electronics.[33] As-synthesized AuNPs required sintering above 400 °C to become conductive due to the relatively high polymer content.[26] TGA was performed to determine the amount of capping agent that was retained after the synthesis and washing steps with nanopure water. Figure 2a shows that the gold NPs had an initial mass loss of ∼10% up to 350 °C, likely due to nonevaporated solvents, and then rapidly increased, losing up to 450 °C, totaling ∼42% mass loss, indicating that the PVP content made up nearly 30% of the total weight of the "dried" sample. A similar trend was also observed in the differential scanning calorimetry (DSC) results of the as-synthesized NPs up to 350 °C. From 350 to 400 °C, multiple exothermic peaks were observed in the DSC results related to the thermal decomposition and sintering of the gold nanoparticles. To reduce the required sintering temperature of the printed constructs, PVP was subsequently washed from the samples using a dilute concentration of sodium borohydride and then repeatedly washed with nanopure water to remove the sodium borohydride and excess PVP from the solution. After the particles were processed to remove PVP, TGA was utilized to determine the amount of capping agent retained after the washing procedure. The processed gold NPs only had a 5.5%

https://doi.org/10.1021/acsmaterialsau.3c00058
ACS Mater. Au 2024, 4, 65–73

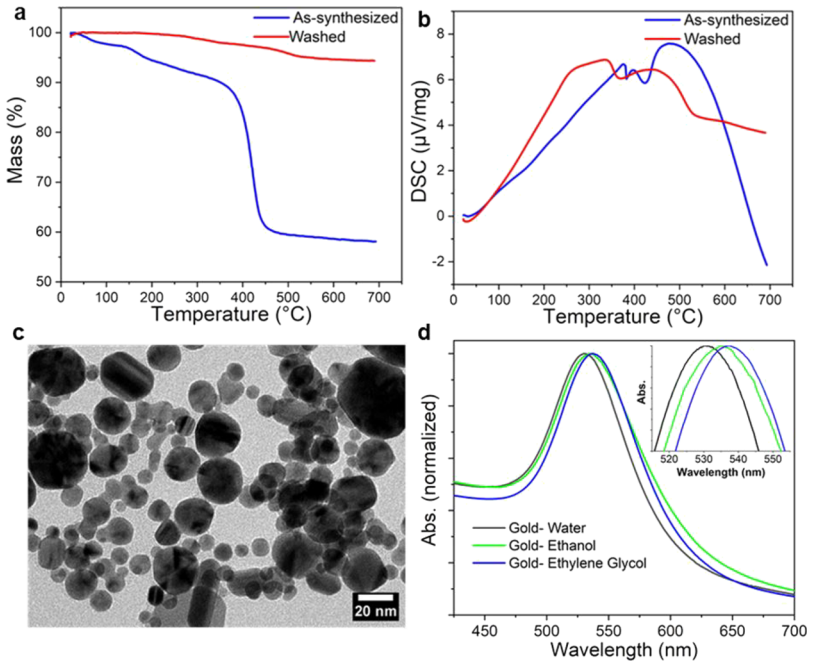

Figure 2. (a) TGA data of as-synthesized fold NPs and after washing steps to remove the retained PVP. The as-synthesized particles had an approximate mass loss of 42%, indicating a significant amount of PVP on the particles, preventing conductivity at temperature below the decomposition temperature of PVP. (b) DSC plots of the as-synthesized and washed gold NPs. (c) TEM image of gold nanoparticles ranging in size from 6 to 50 nm with a spherical to oval morphology. (d) UV−vis absorbance spectra of the gold NPs in water, ethanol, and ethylene glycol. The inset demonstrates a red shift of the surface plasmon response peak position that correlates with an increase of the refractive index of the solvents.

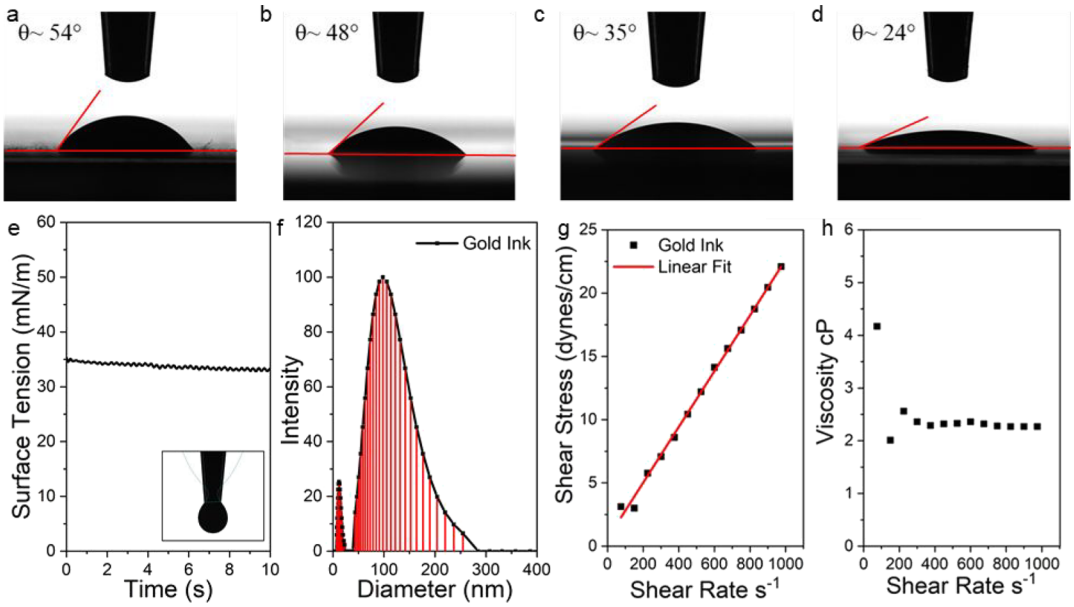

Figure 3. Contact angle images of the washed gold ink droplet on various substrates: (a) tattoo paper, (b) Kapton, (c) PET, and (d) PEL60 paper. Each substrate shows different contact angles, (e) ST pendant drop measurements of Au-NP ink using a tensiometer for 10 s, (f) size distribution of synthesized Au-NPs obtained by DLS measurements, (g) shear stress as a function of shear rate for the nanoparticle ink, and (h) viscosity as a function of shear rate.

mass loss when heated to 700 °C, as shown in the TGA data (Figure 2a), with a significant shift in the DSC peak observed toward lower temperatures. This demonstrated that the majority of the PVP was washed away and indicated potentially lower sintering temperature requirements. This lowering of the sintering temperature is due to the presence of small quantities of PVP, resulting in reduced steric hindrance between the particles and achieving a better thermal transfer between particles. The significantly reduced content of PVP led to low-temperature melting and densifications of the nanoparticles. To evaluate the size and morphology of the gold NPs, TEM was utilized to image the particles. As seen in Figure 2c, the particles ranged from 6 to 50 nm and had a spherical to oval-shaped morphology. This various sizes and morphology are

https://doi.org/10.1021/acsmaterialsau.3c00058
ACS Mater. Au 2024, 4, 65−73

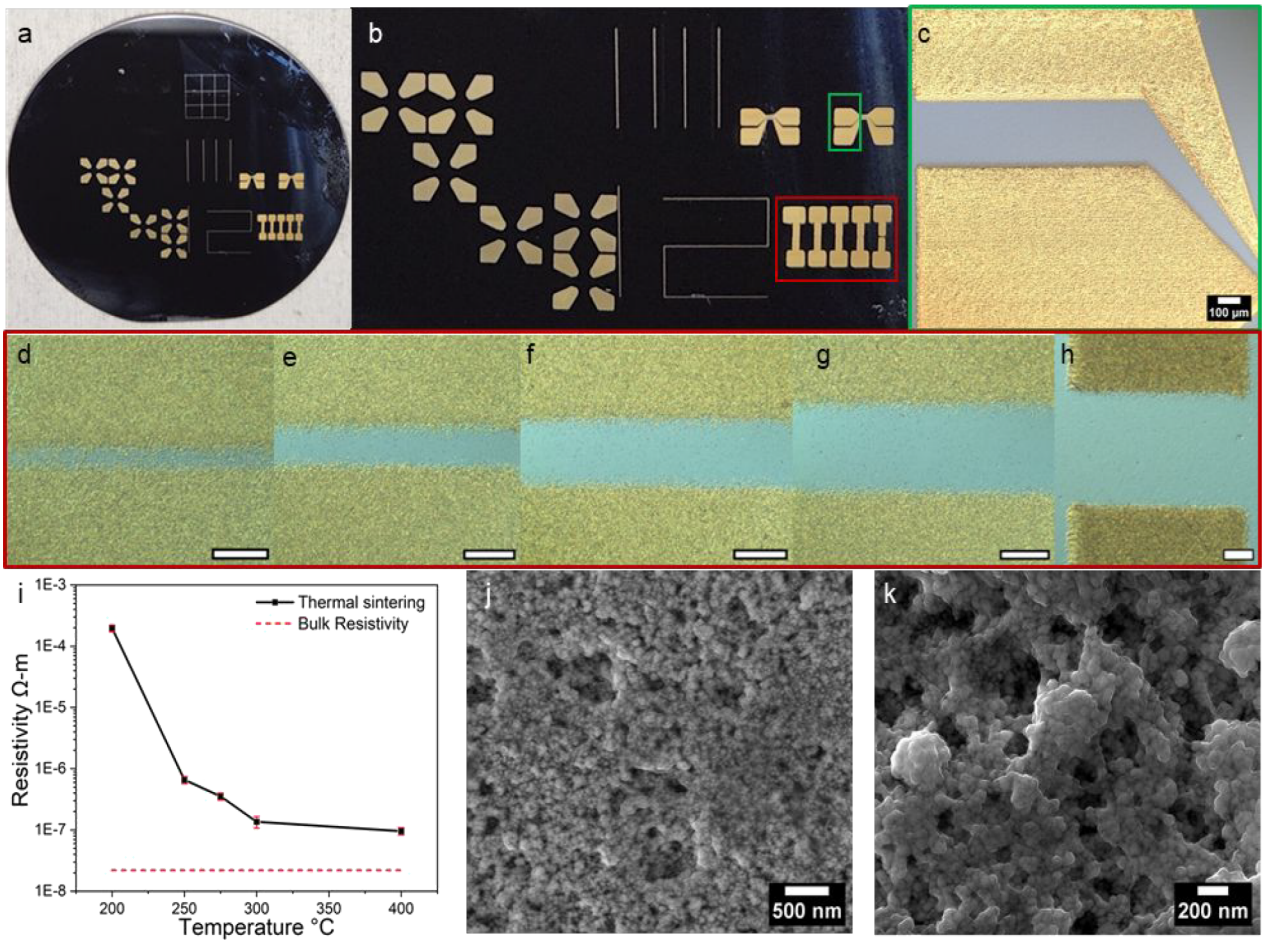

Figure 4. Optical images of printed gold contacts (a) on a 2" silicon wafer with 90 nm silicon oxide, (b and c) optical images of printed gold structures, (d–h) optical images of gold interconnects with varying spacings (scale bar 50 μm) of (d) 25 μm, (e) 50 μm, (f) 100 μm, (g) 150 μm, and (h) 200 μm. (i) Sintering study of printed gold, resistivity as a function of temperature, (j) SEM image of the printed sample, and (k) SEM image of the sintered sample at 400 °C for 45 min.

likely due to PVP preferential adsorption on the {111} facet,[34] manual dropwise addition of the reducing agent, and variations in products from the combination of multiple synthesis batches.

UV–vis was employed to evaluate the size of gold NPs as the surface plasmon resonance (SPR) peak position red shifts with the decreasing size of gold NPs.[35] Multiple batches of the gold NPs were produced and combined to yield the final ink. As the particles are kept in suspension after synthesis and washing procedures, absorbance spectra were obtained for various concentrations of the gold NPs so that Beer's law could be utilized to determine the concentrations of the final ink by using the absorbance intensity of the SPR peak. The UV–vis spectra of the gold NPs (Figure 2d) in different solvents showed the SPR peak position at ∼530.5 nm in water and a systematic red shift of the peak that correlates with an increase in the refractive index of the solvents, as observed in other reports.[36] The peak positions obtained are consistent with the size range obtained from TEM, with a broad peak showing the particle size distribution range of 6–50 nm.

To obtain high-resolution printing and ink formulation with interchangeability between printing modalities, fundamental understanding of the ink rheology and printer parameters are important. The Ohnesorge number (Oh) was used as a numerical indicator to evaluate the general jetting ability of the inks. A relationship between the Reynolds number and the inverse of the Ohnesorge number (Z) is commonly used as a measure for predicting the printability of an ink for inkjet printing.

$$Z = \frac{\sqrt{\gamma \rho D}}{\mu}$$

where Z depends on the surface tension (γ), density (ρ), viscosity (μ), and droplet diameter (D). The droplet diameter, in the case of inkjet printers, depends on the nozzle orifice diameter, which is 21.5 μm. Ink jet printers are capable of forming stable droplets when the Z number is between 1 and 14 by using a cosolvent ink system for Newtonian fluids.[35] Figure S2 shows viscosity, surface tension, and Z number for different combinations of solvent systems, demonstrating precise control over the parameters. Table S1 shows the variation of ink parameters as a function of cosolvent system. After these evaluations, we formulated an ink that consisted of ∼5% gold nanoparticles and utilized a solvent combination of water, ethanol, and ethylene glycol. Since the quality of prints, especially for inkjet printing, relies on ink–substrate interactions, contact angle measurements of the gold nanoinks were conducted on multiple substrates (Figure 3a–d), and the inks demonstrated good wettability in most cases, with the smallest contact angle achieved on PEL 60 paper substrates

https://doi.org/10.1021/acsmaterialsau.3c00058
ACS Mater. Au 2024, 4, 65–73

(24°) and the highest contact angle of 54° on commercial tattoo paper due to the high hydrophobic nature of the PDMS coating. Figure 3f shows the DLS measurements of the nanomaterial inks, showing multiple peaks with average hydrodynamic diameters peaks corresponding to 10 and 100 nm. The multiple peaks are due to the size distribution of nanoparticles in the inks, as shown in the TEM images (Figure 2c). The shear stress-shear rate plot shows a linear relationship that demonstrates Newtonian fluid behavior (Figure 3g). The viscosity-shear rate graph shows a constant value of 2.3 cP over a large shear range with the initial shear thinning behavior due to the low rpm of the spindle. Based on the ink rheology parameters, the ink has a Z number of 12.5 for the ink jet printer and a Reynolds number of 18, meeting the printability window of the inks without forming satellite droplets or splashing. The ternary solvent system used for developing the nanoparticle inks with varying ink viscosity, surface tension (ST), and boiling point helps to control and obtain stable jetting parameters for the inks.

Water (>70%) and ethanol were used for controlling the ST of the ink and increasing the dispersibility of the nanoparticles. Even though the PVP content was greatly reduced from the washing procedures, the hydrophilic nature of the retained PVP-capped AuNPs allows them to be well dispersed in aqueous environments and are stable for many months. Ethylene glycol was utilized for tuning the viscosity of the inks and controlling the Marangoni flow of the droplet to avoid the coffee ring effect. This increases the drying time of the droplet, caused by a slower evaporation rate of the ethylene glycol. The presence of small-scale nanometer particles enables stable printing for long durations without clogging issues, with minimum nozzle cleaning requirements and reducing material waste and cost of printing, as shown in Figure S3.

In the case of aerosol jet printers, the droplet formation happens in the ink vial using an ultrasonic transducer and the jet formation occurs at the nozzle, whereas in an inkjet printer, both droplet formation and jetting occur at the nozzle. A direct comparison of the Ohnesorge number and Reynolds number is not applicable for the aerosol jet printer. In a commercial AJP, an atomizer with a transducer frequency of 1.67 MHz was used to create an aerosol of ink droplets typically 1−5 μm in diameter. For water-based nanomaterial inks, an average mist droplet size of 2.5 μm can be obtained for the aerosolized droplets; the inverse Ohnesorge number Z can be obtained as 4.32.[37] Optimizing the Z number for AJP between 2 and 6 has simultaneously shown to have good jetting properties, equally meeting Z number requirements for ink jet printing.[38] A 300 μm diameter nozzle was used for aerosol jet printing of gold nanomaterial inks with a focusing ratio of two and a speed of 2 mm/s, as shown in Table 1. The print line resolution and the diameter of the aerosol jet stream can be controlled by adjusting the sheath gas to carrier gas ratio, known as the focusing ratio (FR). To control the overspray and obtain high-resolution line prints, the FR ratios were varied from 1 to 2, as shown in Figure S4, for the 150 μm nozzle. As shown in Figure S4, as the focusing ratio increased from 1 to 1.6, the presence of overspray disappeared, and more uniform lines were observed at FR 2. A horseshoe structure was printed using a 150 μm nozzle at a FR2 showing uniform deposition, and Figure S4f shows a magnified image of the horseshoe structure, demonstrating the uniformity of the printed structures. After optimizing the AJP process parameters, gold interconnects are deposited onto a Si/SiO_2 substrate, as shown in Figure 4a−h. The optimized cosolvent system and AJP process parameters created minimum overspray during the atomization process. A higher concentration of smaller droplet in the aerosol tends to promote the drying of droplets during jetting and thereby increases the overspray of the inks due to diffusion and evaporation of smaller droplets into the dry sheath gas.[39] This can be mitigated by increasing the wet fraction of the carrier gas or increasing the high boiling solvent concentration in the ink formulation. Figure 4d−h shows magnified images of the gold contacts with varying channel length ranging from 25 to 250 μm on to a 2 inch silicon wafer. The channels show very sharp edges with minimal overspray up to 50 μm, but in the 25 μm channels, a slight overspray was visible for the 300 μm nozzle diameter. As shown in Figure S4, the line resolution can be further improved to 15 μm without overspray using a 150 μm nozzle and further optimization of the focusing ratio. However, utilizing such a small line resolution is time-consuming when printing larger features.

Four-point probe measurements were conducted on aerosol jet-printed samples to obtain the resistivity of the printed films as a function of sintering temperature, as shown in Figure 4i. Due to the low PVP content of the inks, the resulting prints were conductive without sintering (resistivity = 3.24×10^{-3} Ω m). The resistivity of the nonsintered print was relatively high but significantly reduced after thermal treatment. The resistivity of the printed samples sintered at 200 °C for 45 min showed a resistivity of $2.0 \pm 0.25 \times 10^{-4}$ Ω m. The resistivity further reduced by 3 orders of magnitude when the sintering temperature increased from 200 to 250 °C and reached the lowest value at 400 °C ($9.6 \pm 1.25 \times 10^{-8}$ Ω m). At 400 °C, the resistivity of the printed gold was only four times the bulk resistivity of gold for thin films having a thickness of 400 nm. The rapid decrease in electrical resistivity at 250 °C is due to the low concentration of PVP present in the ink and also due to the size-dependent melting point depression of the nanoparticles, as observed in DSC and TEM data (Figure 2b). Figure 4j,k shows surface SEM images of the printed structures on a glass substrate. Figure 4j shows that the as-printed films have a loosely packed structure and a large number of pores. As the temperature increased, smaller nanoparticles began to melt and bind the bigger nanoparticles together, creating a more continuous and dense film as seen in Figure 4k. The melting and subsequent necking of the nanoparticles are clearly visible in the SEM image of the printed films sintered at 400 °C for 45 min. To understand the ink−substrate interactions, multijet gold inks were deposited onto a variety flexible and solid substrates using both an inkjet printer and an aerosol jet printer as shown in Figure S6. Gold nanoparticles inks are highly desirable for printed electronics as well as wearable applications. The ink shows good deposition and wetting proprieties onto multiple commercial polymers including HN-polyimide, PEL60 paper substrates, and transparent polymers such as PET and PEN, presenting exciting prospects for the field of printed and wearable technologies. Similarly, Table S2 shows a comparative performance of this work with literature data as well as commercially available gold nanoparticle inks. Among the reported AuNP inks, this work is the only ink reported to be compatible with both aerosol and ink jet printers simultaneously, achieving high electrical conductivities with very small weight percentage of gold nanoparticles in the ink formulations, reducing the cost of nanomaterials in the ink as well as sustainable manufacturing of

https://doi.org/10.1021/acsmaterialsau.3c00058
ACS Mater. Au 2024, 4, 65−73

gold nanoparticle inks for wearable and printed electronic applications.

CONCLUSIONS

In this work, we have demonstrated a scalable manufacturing and ink formulation for multiprinter compatible gold inks. We have demonstrated that removing the excess capping agents and optimizing the solvent combinations along with optimizing process parameters can create high-resolution lines (<20 μm). Removing excess surfactant present on the material can significantly reduce the required sintering temperature of the printed films, achieving resistivity as low as $9.6 \pm 1.25 \times 10^{-8}$ Ω m at 400 °C for film thickness as low as 400 nm. Selecting a three-solvent system with different viscosities, surface tension, and boiling points offers fine control of the ink properties and Ohnesorge number of the ink while making the ink cross compatible with both ink jet and aerosol jet printers. High-resolution and high-quality print lines can be obtained by controlling the focusing ratio of the AJP print nozzles. Finally, this demonstrates a low-cost and low-temperature sintering gold nanomaterial ink formulation that is compatible with both aerosol jet printing and ink jet printing for highly conductive printed electronic applications.

ASSOCIATED CONTENT

Supporting Information

The Supporting Information is available free of charge at https://pubs.acs.org/doi/10.1021/acsmaterialsau.3c00058.

Additional experimental details including nanoparticle reduction mechanism, rheological properties of solvent combinations, Marangoni and coffee ring studies on ink jet-printed droplet, focusing ratio optimization for aerosol jet printing and both ink jet and aerosol jet-printed structures on multiple substrates, and comparative performance of gold nanomaterial inks (PDF)

AUTHOR INFORMATION

Corresponding Authors

Tony Valayil Varghese − *Department of Electrical and Computer Engineering and Micron School of Material Science and Engineering, Boise State University, Boise, Idaho 83725, United States*; Email: tonyvalayilvarghese@boisestate.edu

David Estrada − *Micron School of Material Science and Engineering, Center for Atomically Thin Multifunctional Coatings, and Center for Advanced Energy Studies, Boise State University, Boise, Idaho 83725, United States; School of Science, Department of Chemistry and Biotechnology, Tallinn University of Technology, 19086 Tallinn, Estonia; Inflex Laboratories LLC, Boise, Idaho 83706, United States;* orcid.org/0000-0001-5894-0773; Email: daveestrada@boisestate.edu

Authors

Josh Eixenberger − *Micron School of Material Science and Engineering, Department of Physics, Center for Atomically Thin Multifunctional Coatings, and Center for Advanced Energy Studies, Boise State University, Boise, Idaho 83725, United States;* orcid.org/0000-0002-9816-7268

Fereshteh Rajabi-Kouchi − *Micron School of Material Science and Engineering, Boise State University, Boise, Idaho 83725, United States*

Maryna Lazouskaya − *Micron School of Material Science and Engineering, Boise State University, Boise, Idaho 83725, United States; Idaho National Laboratory, Idaho Falls, Idaho 83415, United States*

Cadré Francis − *Micron School of Material Science and Engineering, Boise State University, Boise, Idaho 83725, United States*

Hailey Burgoyne − *Micron School of Material Science and Engineering, Boise State University, Boise, Idaho 83725, United States*

Katelyn Wada − *Micron School of Material Science and Engineering, Boise State University, Boise, Idaho 83725, United States*

Harish Subbaraman − *School of Electrical Engineering and Computer Science, Oregon State University, Corvallis, Oregon 97331, United States; Inflex Laboratories LLC, Boise, Idaho 83706, United States*

Complete contact information is available at: https://pubs.acs.org/10.1021/acsmaterialsau.3c00058

Author Contributions

T.V., J.E., and D.E. conceptualized the experiments. T.V. and J.E. synthesized, processed, and characterized the gold NPs. T.V. executed the ink formulation studies, characterized and printed the inks, characterized printed devices, and analyzed the data with support from F.RK., M.L., K.W., C.F., and H.B. T.V., and J.E. drafted the manuscript with assistance from D.E. and H.S. D.E directed the project. All coauthors provided inputs and comments on the manuscript. CRediT: **Tony Valayil Varghese** conceptualization, funding acquisition, investigation, project administration, writing-review & editing; **David Estrada** conceptualization, funding acquisition, investigation, project administration, resources, supervision, writing-review & editing.

Funding

This work was supported in part by the Idaho Commerce IGEM (award# 3732018) based on research sponsored by the Air Force Research Laboratory (AFRL) under Agreement Number FA8650-20-2-5506. The U.S. Government is authorized to reproduce and distribute reprints for Governmental Purposes notwithstanding any copyright notation thereon.

Notes

The authors declare the following competing financial interest(s): D.E. and H.S. declare competing interests with INFlex Labs, LLC, the company commercializing multijet gold inks.

ACKNOWLEDGMENTS

The authors acknowledge infrastructure support in part through the Department of Energy Advanced Sensors and Instrumentation program under DOE Idaho Operations Office Contract DE-AC07-05ID14517. We acknowledge infrastructure support from the Department of Energy Nuclear Science User Facilities General Infrastructure Program through award numbers DE-NE0008677 and DE-NE0008496. M.L. acknowledges the support from the European Regional Development fund and the Republic of Estonia via the Dora Plus mobility scholarships. The views and opinions of authors expressed herein do not necessarily state or reflect those of the U.S. Government or any agency thereof. We also support

infrastructure from the Center for Advanced Energy Studies, the Idaho Global Entrepreneurship Mission, the Micron Foundation, and the M. J. Murdock Charitable Trust.

REFERENCES

(1) Chang, J.; He, J.; Mao, M.; Zhou, W.; Lei, Q.; Li, X.; Li, D.; Chua, C.-K.; Zhao, X. Advanced Material Strategies for Next-Generation Additive Manufacturing. *Materials* **2018**, *11* (1), 10166.
(2) Hirt, L.; Reiser, A.; Spolenak, R.; Zambelli, T. Additive Manufacturing of Metal Structures at the Micrometer Scale. *Adv. Mater.* **2017**, *29* (17), No. 1604211.
(3) Murphy, S. V.; Atala, A. 3D Bioprinting of Tissues and Organs. *Nat. Biotechnol.* **2014**, *32* (8), 773−785.
(4) Fantino, E.; Chiappone, A.; Roppolo, I.; Manfredi, D.; Bongiovanni, R.; Pirri, C. F.; Calignano, F. 3D Printing of Conductive Complex Structures with In Situ Generation of Silver Nanoparticles. *Adv. Mater.* **2016**, *28* (19), 3712−3717.
(5) Narupai, B.; Nelson, A. 100th Anniversary of Macromolecular Science Viewpoint: Macromolecular Materials for Additive Manufacturing. *ACS Macro Lett.* **2020**, *9* (5), 627−638.
(6) Han, D.; Lee, H. Recent Advances in Multi-Material Additive Manufacturing: Methods and Applications. *Curr. Opin. Chem. Eng.* **2020**, *28*, 158−166.
(7) Manzi, J.; Weltner, A. E.; Varghese, T.; McKibben, N.; Busuladzic-Begic, M.; Estrada, D.; Subbaraman, H. Plasma-Jet Printing of Colloidal Thermoelectric Bi2Te3 Nanoflakes for Flexible Energy Harvesting. *Nanoscale* **2023**, *15* (14), 6596−6606.
(8) Ibrahim, N.; Akindoyo, J. O.; Mariatti, M. Recent Development in Silver-Based Ink for Flexible Electronics. *J. Sci. Adv. Mater. Devices* **2022**, *7* (1), 100395.
(9) Kipphan, H. Printing Technologies without a Printing Plate (NIP Technologies). In *Handbook of Print Media: Technologies and Production Methods*; Kipphan, H., Ed.; Springer Berlin Heidelberg: Berlin, Heidelberg, 2001; pp 675−758.
(10) Kipphan, H. Printing Technologies with Permanent Printing Master. In *Handbook of Print Media: Technologies and Production Methods*; Kipphan, H., Ed.; Springer Berlin Heidelberg: Berlin, Heidelberg, 2001; pp 203−448.
(11) Saengchairat, N.; Tran, T.; Chua, C.-K. A Review: Additive Manufacturing for Active Electronic Components. *Virtual Phys. Prototyp.* **2017**, *12* (1), 31−46.
(12) Khan, S.; Lorenzelli, L.; Dahiya, R. S. Technologies for Printing Sensors and Electronics Over Large Flexible Substrates: A Review. *IEEE Sens. J.* **2015**, *15* (6), 3164−3185.
(13) Idrees, M.; Batool, S.; Din, M. A. U.; Javed, M. S.; Ahmed, S.; Chen, Z. Material-Structure-Property Integrated Additive Manufacturing of Batteries. *Nano Energy* **2023**, *109*, No. 108247.
(14) Derby, B. Inkjet Printing of Functional and Structural Materials: Fluid Property Requirements, Feature Stability, and Resolution. *Annu. Rev. Mater. Res.* **2010**, *40*, 395−414.
(15) Molina-Lopez, F.; Gao, T. Z.; Kraft, U.; Zhu, C.; Öhlund, T.; Pfattner, R.; Feig, V. R.; Kim, Y.; Wang, S.; Yun, Y.; Bao, Z. Inkjet-Printed Stretchable and Low Voltage Synaptic Transistor Array. *Nat. Commun.* **2019**, *10* (1), 2676.
(16) Song, O.; Rhee, D.; Kim, J.; Jeon, Y.; Mazánek, V.; Söll, A.; Kwon, Y. A.; Cho, J. H.; Kim, Y.-H.; Sofer, Z.; Kang, J. All Inkjet-Printed Electronics Based on Electrochemically Exfoliated Two-Dimensional Metal, Semiconductor, and Dielectric. *npj 2D Mater. Appl.* **2022**, *6* (1), 64.
(17) Cho, K.; Lee, T.; Chung, S. Inkjet Printing of Two-Dimensional van Der Waals Materials: A New Route towards Emerging Electronic Device Applications. *Nanoscale Horiz.* **2022**, *7* (10), 1161−1176.
(18) Yan, K.; Li, J.; Pan, L.; Shi, Y. Inkjet Printing for Flexible and Wearable Electronics. *APL Mater.* **2020**, *8* (12), 31669.
(19) He, P. *Inkjet Printing of Two Dimensional Materials A Thesis Submitted to the*; University of Manchester, 2016.
(20) Simon, J. C.; Sapozhnikov, O. A.; Khokhlova, V. A.; Crum, L. A.; Bailey, M. R. Ultrasonic Atomization of Liquids in Drop-Chain Acoustic Fountains. *J. Fluid Mech.* **2015**, *766*, 129−146.
(21) Sadie, J. *Three-Dimensional Inkjet-Printed Metal Nanoparticles: Ink and Application Development*; University of California: Berkeley, 2017. http://www2.eecs.berkeley.edu/Pubs/TechRpts/2017/EECS-2017-168.pdf.
(22) Park, Y.-G.; Yun, I.; Chung, W. G.; Park, W.; Lee, D. H.; Park, J.-U. High-Resolution 3D Printing for Electronics. *Adv. Sci.* **2022**, *9* (8), No. 2104623.
(23) Joshi, P. C.; Dehoff, R. R.; Duty, C. E.; Peter, W. H.; Ott, R. D.; Love, L. J.; Blue, C. A. Direct Digital Additive Manufacturing Technologies: Path towards Hybrid Integration. In *2012 Future of Instrumentation International Workshop (FIIW) Proceedings*, 2012; pp 1−4.
(24) Skarżyński, K.; Krzemiński, J.; Jakubowska, M.; Słoma, M. Highly Conductive Electronics Circuits from Aerosol Jet Printed Silver Inks. *Sci. Rep.* **2021**, *11* (1), 18141.
(25) Ali, M. A.; Hu, C.; Yuan, B.; Jahan, S.; Saleh, M. S.; Guo, Z.; Gellman, A. J.; Panat, R. Breaking the Barrier to Biomolecule Limit-of-Detection via 3D Printed Multi-Length-Scale Graphene-Coated Electrodes. *Nat. Commun.* **2021**, *12* (1), 7077.
(26) Pandhi, T.; Cornwell, C.; Fujimoto, K.; Barnes, P.; Cox, J.; Xiong, H.; Davis, P. H.; Subbaraman, H.; Koehne, J. E.; Estrada, D. Fully Inkjet-Printed Multilayered Graphene-Based Flexible Electrodes for Repeatable Electrochemical Response. *RSC Adv.* **2020**, *10* (63), 38205−38219.
(27) Pandhi, T.; Kreit, E.; Aga, R.; Fujimoto, K.; Sharbati, M. T.; Khademi, S.; Chang, A. N.; Xiong, F.; Koehne, J.; Heckman, E. M.; Estrada, D. Electrical Transport and Power Dissipation in Aerosol-Jet-Printed Graphene Interconnects. *Sci. Rep.* **2018**, *8* (1), 10842.
(28) Zhang, C. J.; McKeon, L.; Kremer, M. P.; Park, S.-H.; Ronan, O.; Seral-Ascaso, A.; Barwich, S.; Coileáin, C. Ó.; McEvoy, N.; Nerl, H. C.; Anasori, B.; Coleman, J. N.; Gogotsi, Y.; Nicolosi, V. Additive-Free MXene Inks and Direct Printing of Micro-Supercapacitors. *Nat. Commun.* **2019**, *10* (1), 1795.
(29) Liu, Y.; Xie, J.; Liu, L.; Fan, K.; Zhang, Z.; Chen, S.; Chen, S. Inkjet-Printed Highly Conductive Poly(3,4-Ethylenedioxythiophene): Poly(Styrenesulfonate) Electrode for Organic Light-Emitting Diodes. *Micromachines* **2021**, *12* (8), 80889.
(30) Tarabella, G.; Vurro, D.; Lai, S.; D'Angelo, P.; Ascari, L.; Iannotta, S. Aerosol Jet Printing of PEDOT:PSS for Large Area Flexible Electronics. *Flex. Print. Electron.* **2020**, *5* (1), 14005.
(31) Kim, F.; Connor, S.; Song, H.; Kuykendall, T.; Yang, P. Platonic Gold Nanocrystals. *Angew. Chem., Int. Ed. Engl.* **2004**, *43* (28), 3673−3677.
(32) Kang, H.; Buchman, J. T.; Rodriguez, R. S.; Ring, H. L.; He, J.; Bantz, K. C.; Haynes, C. L. Stabilization of Silver and Gold Nanoparticles: Preservation and Improvement of Plasmonic Functionalities. *Chem. Rev.* **2019**, *119* (1), 664−699.
(33) Yokoyama, S.; Nozaki, J.; Motomiya, K.; Tsukahara, N.; Takahashi, H. Strong Adhesion of Polyvinylpyrrolidone-Coated Copper Nanoparticles on Various Substrates Fabricated from Well-Dispersed Copper Nanoparticle Inks. *Colloids Surf., A* **2020**, *591*, No. 124567.
(34) Liu, S.-H.; Saidi, W. A.; Zhou, Y.; Fichthorn, K. A. Synthesis of {111}-Faceted Au Nanocrystals Mediated by Polyvinylpyrrolidone: Insights from Density-Functional Theory and Molecular Dynamics. *J. Phys. Chem. C* **2015**, *119* (21), 11982−11990.
(35) Sørensen, L. K.; Khrennikov, D. E.; Gerasimov, V. S.; Ershov, A. E.; Polyutov, S. P.; Karpov, S. V.; Ågren, H. Nature of the Anomalous Size Dependence of Resonance Red Shifts in Ultrafine Plasmonic Nanoparticles. *J. Phys. Chem. C* **2022**, *126* (39), 16804−16814.
(36) Ghosh, S. K.; Nath, S.; Kundu, S.; Esumi, K.; Pal, T. Solvent and Ligand Effects on the Localized Surface Plasmon Resonance (LSPR) of Gold Colloids. *J. Phys. Chem. B* **2004**, *108* (37), 13963−13971.

https://doi.org/10.1021/acsmaterialsau.3c00058
ACS Mater. Au 2024, 4, 65−73

(37) Feng, J. Q.; Renn, M. J. Aerosol Jet® Direct-Write for Microscale Additive Manufacturing. *J. Micro Nano-Manufacturing* **2019**, *7* (1), 1−7.
(38) Ramesh, S.; Mahajan, C.; Gerdes, S.; Gaikwad, A.; Rao, P.; Cormier, D. R.; Rivero, I. V. Numerical and Experimental Investigation of Aerosol Jet Printing. *Addit. Manuf.* **2022**, *59*, No. 103090.
(39) Secor, E. B. Guided Ink and Process Design for Aerosol Jet Printing Based on Annular Drying Effects. *Flex. Print. Electron.* **2018**, *3* (3), No. 035007.

https://doi.org/10.1021/acsmaterialsau.3c00058
ACS Mater. Au 2024, 4, 65−73